Targeting Phosphatidylserine with Calcium-dependent Protein-Drug Conjugates for the Treatment of Cancer

Ran Li[1], Srinivas Chiguru[2], Li Li[2], Dongyoung Kim[3], Ramraj Velmurugan[1,4], David Kim[3], Siva Charan Devanaboyina[1], Hong Tian[5], Alan Schroit[6], Ralph Mason[2], Raimund J. Ober[1,3] and E. Sally Ward[1,7]

[1]Department of Molecular and Cellular Medicine, Texas A&M University Health Science Center, College Station, Texas, United States.

[2]Department of Radiology, University of Texas Southwestern Medical Center, Dallas, TX, United States.

[3]Department of Biomedical Engineering, Texas A&M University, College Station, Texas, United States.

[4]Biomedical Engineering Graduate Program, University of Texas Southwestern Medical Center, Dallas, TX, United States.

[5]China Pharmaceutical University, Nanjing, Jiangsu, China (current address).

[6]Department of Pharmacology, University of Texas Southwestern Medical Center, Dallas, TX, United States.

[7]Department of Microbial Pathogenesis and Immunology, Texas A&M University Health Science Center, College Station, Texas, United States.

Running Title: Cancer Targeting with Ca^{2+}-dependent Protein-Drug Conjugates

Keywords: Phosphatidylserine, Antibody, Drug-Conjugate, Calcium-dependent, Cancer Therapy

Corresponding Author: E. Sally Ward, Department of Molecular and Cellular Medicine, Texas A&M University Health Science Center, 469 Joe H. Reynolds Medical Sciences Building, 1114 TAMU, College Station, TX 77843, USA. Phone: 979-436-0742; Email: sally.ward@medicine.tamhsc.edu

Financial Information:

This study was supported in part by grants from the Cancer Prevention and Research Institute of Texas (CPRIT; RP 110441, awarded to E. S. Ward, R. J. Ober, A. Schroit and R. Mason) and the National Institutes of Health (Simmons Comprehensive Cancer Center support grant; 5P30CA142543, awarded to M. Cobb). The IVIS Spectrum was purchased with support (1S10RR024757, awarded to R. Mason) from the National Institutes of Health.

Abstract

In response to cellular stress, phosphatidylserine (PS) is exposed on the outer membrane leaflet of tumor blood vessels and cancer cells, motivating the development of PS-specific therapies. The generation of drug-conjugated PS-targeting agents represents an unexplored therapeutic approach, for which anti-tumor effects are critically dependent on efficient internalization and lysosomal delivery of the cytotoxic drug. In the current study, we have generated PS-targeting agents by fusing PS-binding domains to a human IgG1-derived Fc fragment. The tumor localization and pharmacokinetics of several PS-specific Fc fusions have been analyzed in mice and demonstrate that Fc-Syt1, a fusion containing the synaptotagmin 1 C2A domain, effectively targets tumor tissue. Conjugation of Fc-Syt1 to the cytotoxic drug, monomethyl auristatin E, results in a protein-drug conjugate (PDC) that is internalized into target cells and, due to the Ca^{2+}-dependence of PS binding, dissociates from PS in early endosomes. The released PDC is efficiently delivered to lysosomes and has potent anti-tumor effects in mouse xenograft tumor models. Interestingly, whilst an engineered, tetravalent Fc-Syt1 fusion shows increased binding to target cells, this higher avidity variant demonstrates reduced persistence and therapeutic effects compared with bivalent Fc-Syt1. Collectively, these studies show that finely tuned, Ca^{2+}-switched PS-targeting agents can be therapeutically efficacious.

Introduction

The use of antibody-based targeted therapies for cancer has greatly expanded over the past two decades. However, almost all antibody-based agents target protein receptors that are present at higher levels on tumors compared with normal tissue. Whilst many tumor cells and the tumor vascular endothelium (1-3) specifically expose the negatively-charged phospholipid, phosphatidylserine (PS), in their outer membrane leaflet, few studies have taken advantage of PS as a therapeutic target (4).

The identification of PS as a tumor marker has prompted the development of molecular targeted therapies specific for this phospholipid. Amongst these therapeutics is bavituximab, a chimeric monoclonal antibody that targets the PS-binding serum protein β2 glycoprotein-1 (β2GP1) (5). By cross-linking β2GP1, bavituximab binds PS indirectly with high affinity and elicits anti-angiogenic effects via antibody-dependent cell-mediated cytotoxicity (ADCC) (6). In addition, by masking PS in the tumor microenvironment, bavituximab might also play an immunomodulatory role by inducing polarization of macrophages to the inflammatory M1 phenotype and reducing the number of myeloid-derived suppressor cells (7). In combination with radiation or chemotherapy, bavituximab has been demonstrated to be effective in multiple preclinical models for glioblastoma, pancreatic cancer, prostate, breast and hepatocellular carcinomas (6-10). However, a recent phase III clinical trial (NCT01999673; http://www.peregrineinc.com/pipeline/bavituximab-oncology.html) in non-small cell lung cancer patients was discontinued since bavituximab in combination with docetaxel did not show sufficient improvement in overall survival over treatment with docetaxel alone. This motivates the development of strategies to improve the *in vivo* anti-tumor activity of PS-targeting therapies.

Antibody-drug conjugates (ADCs) combine the high specificity of antibody targeting with potent cytotoxic drugs and promise to be more effective in killing tumor cells than their corresponding 'naked' antibodies (11,12). To date, three ADCs (Mylotarg, Adcetris and Kadcyla) have received regulatory approval, although Mylotarg has been withdrawn (11). More than 50 other ADCs are in clinical development (13,14). This suggests that a PS-specific ADC may have improved efficacy over naked PS-targeting antibodies such as bavituximab. However, the generation of a PS-specific ADC faces several challenges. First, following binding to the cell surface, ADCs require effective internalization into the lysosomal pathway. The internalization behavior of PS and its subsequent trafficking has not been explored. Second, by contrast with protein antigens, the development of high affinity, specific antibodies to small molecule "haptens" such as PS is challenging (bavituximab targets PS indirectly through binding to β2GP1). Third, under certain circumstances PS can also be exposed on the surface of non-apoptotic cells, such as differentiating monocytes and a subpopulation of T cells (15-17).

To generate an effective PS-directed drug conjugate, we produced a panel of PS-targeting agents by fusing naturally occurring PS-binding domains to the Fc portion of human IgG1. To achieve efficient dissociation of the targeting agents from PS in sorting (early) endosomes, followed by their lysosomal delivery, we have exploited the significant decrease in Ca^{2+} levels in endosomes (18,19) by using PS-binding domains that interact with PS in a Ca^{2+}-dependent manner. We initially analyzed the pharmacokinetics and tumor targeting of the PS-targeting agents in mice, and observed that despite its relatively low affinity for PS binding, a fusion comprising the C2A domain of synaptotagmin 1 (Fc-Syt1) had superior properties compared with higher affinity protein kinase C-α (PKCα)- and Annexin A1 (AnxA1)-based fusions. Fc-Syt1 was therefore used as a platform to generate a protein-drug conjugate (PDC) with monomethyl auristatin E (MMAE). Modulation of the avidity of Fc-Syt1 for PS binding demonstrated that a bivalent Fc-Syt1-based PDC had improved therapeutic efficacy over a tetravalent variant due to

more favorable pharmacokinetic properties. Our observations indicate the need for affinity/avidity tuning of PS-targeting PDCs and provide novel insight into the design of therapeutics to target this phospholipid.

Materials and Methods

Cell lines and culture conditions

2H11 mouse tumor endothelial cells (ATCC, CRL-2163) and MDA-MB-231 human breast cancer cells (ATCC, HTB-26) were cultured in Dulbecco's modified Eagle's medium (DMEM) supplemented with 5% and 10% fetal bovine serum (FBS), respectively. T-47D breast cancer cells (ATCC, HTB-133) and LNCaP and 22Rv1 human prostate cancer cells (ATCC, CRL-1740 and CRL-2505) were cultured in RPMI 1640 medium supplemented with 10% FBS. SK-BR-3 human breast cancer cells (ATCC, HTB-30) were cultured in McCoy's 5A medium supplemented with 10% FBS. All cell lines were authenticated with DNA fingerprinting by the University of Arizona Genetics Core (UAGC) on November 16, 2016 and tested for *Mycoplasma* at monthly intervals. All cell lines were used within 15 passages following thawing of master stocks. Cells were cultured at 37°C with 5% CO_2. Expi293F cells were used for protein expression and were cultured in Expi293 expression medium (Life Technologies, catalog number A14635) at 37°C with 8% CO_2 and 80% humidity.

Antibodies

The following antibodies were used in this study: rat anti-mouse LAMP1, mouse anti-human LAMP1 and mouse anti-beta tubulin antibodies (Developmental Studies Hybridoma Bank, clone # 1D4B, H4A3 and E7); mouse anti-human EEA1 and rat anti-mouse CD31 antibodies (BD Biosciences, catalog # 610456 and 557355); goat anti-human IgG (H+L) antibody conjugated with HRP, donkey anti-rat (H+L) antibody conjugated with Alexa Fluor 488 and donkey anti-human IgG (H+L) antibody conjugated with Cy3 (Jackson ImmunoResearch, catalog # 109-035-003, 712-545-153 and 709-165-149); goat anti-human IgG (H+L) antibody conjugated with Alexa Fluor 555, goat anti-mouse IgG (H+L) antibody conjugated with Alexa Fluor 488 and goat

anti-human IgG (H+L) antibody conjugated with Alexa Fluor 647 (Life Technologies, catalog # A21433, A11029 and A21445); rabbit anti-human Ki-67 antibody (Abcam, catalog # 92742).

Protein labeling

Proteins were labeled with Alexa 647 or IRDye800CW with the Alexa Fluor 647 NHS Ester (Life Technologies, catalog # A37573) or IRDye800CW protein labeling kit (LI-COR, catalog # 928-38040), respectively, following the manufacturer's instructions. Proteins were labeled with I-125 as described previously (20). Radio-TLC analysis was used to determine radioiodination efficiency and radiochemical purity using a Rita Star Radioisotope TLC Analyzer (Straubenhardt, Germany) with ITLC-SG plates and PBS as the mobile phase. The typical radiochemical yield was 68-76%, with radiochemical purity (RCY) of > 99.5% and specific activity of 10-12 µCi/µg. The absence of aggregation for fluorophore-labeled proteins was verified by gel filtration analyses.

Generation of expression constructs

For use as controls, the Fc region including the hinge region (residues 214-446 of the heavy chain) of the hen egg lysozyme-specific human IgG1, HuLys10 (21), was cloned into the pcDNA3.4 vector with the N-terminal leader peptide derived from a mouse IgG heavy chain (21,22). Similarly, the genes encoding the heavy and light chain genes (cDNA) of the HuLys10 antibody were cloned into pcDNA3.4. For the control IgG heavy and light chain constructs, Cys214 in the light chain, which forms a sulphydryl bridge with Cys219 in the heavy chain of HuLys10 were both mutated to serine residues using the QuikChange II Site-Directed Mutagenesis Kit (Agilent Technologies, catalog # 200523).

cDNA clones for human Annexin A1 (AnxA1), human synaptotagmin 1 (Syt1) and human PKCα were purchased from Open Biosystems (clone ID: 3459615, clone ID: 6187902 and clone ID:

40028305, respectively). Genes encoding the AnxA1 PS-binding core domain (amino acids 41-346), the Syt1 PS-binding C2A domain (amino acids 141-266) and PKCα PS-binding C2 domain (amino acids 157-288) were fused via a Gly_4Ser linker sequence to the CH_3 domain of the human IgG1 Fc region (residues 214-446) with a leader peptide derived from the mouse IgG heavy chain (21,22). Cys219 in the hinge region was mutated in all Fc fusion constructs so that there are two cysteine residues per hinge. The genes encoding the Fc fusions were cloned into the pcDNA3.4 vector (Invitrogen, catalog # 14308).

To generate Syt1-Fc-Syt1, the Syt1 PS-binding C2A domain (amino acids 141-266) was linked to the N-terminus of the hinge region of the Fc-Syt1 construct via a Gly_4Ser linker sequence. The leader peptide derived from a mouse IgG heavy chain (21,22) was appended to the N-terminus of the hinge-linked Syt1 PS-binding C2A domain, and the resulting Fc fusion was cloned into the pcDNA3.4 vector. Mutations to reduce PS-binding of the Syt1 C2A domain (D173N, D179N, D231N, D233N and D239N) (23) were inserted in the Fc-Syt1 construct to generate Fc-Syt1(DN) and cloned into the pcDNA3.4 vector. All constructs were generated using standard methods of molecular biology and designed oligonucleotides. Following construction of expression plasmids, sequences were verified. Oligonucleotide and construct sequences are available upon request.

Protein expression and purification

All PS-targeting proteins used in this study were produced using the Expi293 expression system from Life Technologies following the manufacturer's instructions. Briefly, cells were transfected with expression constructs for 6-7 days and Fc fusion proteins were purified from culture supernatants using protein G-Sepharose. Bound proteins were eluted using 50 mM diethylamine with 150 mM NaCl. The eluted protein was neutralized using 2M Tris pH 7.0 followed by dialysis against PBS. All proteins were concentrated and loaded onto a Hiload 16/60

Superdex 200 gel filtration column (GE Healthcare). The homodimeric, non-aggregated form of the protein was separated, concentrated and analyzed using a Superdex 200 15/30 gel filtration column (GE Healthcare).

Recombinant mouse FcRn was produced as previously described (24). Briefly, High Five cells grown at 27°C in EX-CELL 405 medium (Sigma, catalog # 14405) were infected at a density of 1 x 10^6 cells/ml with recombinant baculovirus (mouse FcRn α-chain/mouse β2-microglobulin). Cells were cultured at 23–24°C for 72 hours. Mouse FcRn was purified from the supernatant using Ni^{2+}-NTA agarose (Qiagen) followed by the use of a Hiload 16/60 Superdex 200 gel filtration column.

MALDI-TOF mass spectrometry

For MALDI-TOF analyses, all samples (20-40 µg diluted in 20 µl PBS) were treated with 1 µl (10 U) PNGase F (Promega, catalog # V4831) at 37°C for 1 hour. Samples were extracted using C_4 LithTips (Protea, catalog # SP-410) and analyzed with sinapic acid under linear conditions with a Kratos/Shimadzu Axima CFR MALDI-TOF mass spectrometer.

Surface plasmon resonance (BIAcore) analyses

Surface plasmon resonance experiments were carried out using a BIAcore T200 (GE Healthcare). To determine the equilibrium binding affinities of mouse FcRn for the PS-targeting agents (Fc-AnxA1, Fc-Syt1 and Fc-PKCα), control human IgG1 and Fc, mouse FcRn was injected over immobilized proteins (coupled at ~ 750 - 1500 RU on flow cells of CM5 sensor chips) at a flow rate of 10 µl/minute in PBS (pH 6.0) with 0.01% v/v Tween 20. Flow cells were regenerated at the end of each run using 0.15 M NaCl, 0.1 M $NaHCO_3$, pH 8.5. The dissociation constants (K_Ds) for the interactions of mouse FcRn with different proteins were determined

using custom written software (25,26). IgG or Fc has two possible interaction sites on mouse FcRn, and equilibrium binding data were fitted as described previously (26). The equilibrium dissociation constants for the higher affinity interaction site are reported.

Membrane lipid strip binding assay

Lipid-coated membrane strips (Echelon, catalog # P-6002) were first hydrated with TBST (20 mM Tris, 150 mM NaCl, 0.1% Tween 20, pH 7.5) and then incubated with blocking solution (4% fatty acid free BSA dissolved in TBST) at room temperature for 1 hour. Proteins were diluted to a concentration of 2 µg/ml in blocking buffer and incubated with membranes at room temperature for 2 hours. The lipid strip was then washed with TBST and bound proteins detected using HRP-conjugated goat anti-human IgG (H+L) antibody.

Fluorescence microscopy analyses

2H11 or MDA-MB-231 cells were grown on coverslips (Zeiss, ref # 0109030091) and incubated with either control human IgG1 (HuLys10) or PS-specific agents diluted in growth medium for the indicated time points in figure legends. Cells were then washed with PBS and fixed with ice-cold 4% PFA at room temperature for 20 minutes. Following fixation, cells were permeabilized with 0.1% Triton X-100 and incubated with blocking buffer (PBS, 0.1% Tween 20, 5% serum) at room temperature for 30 minutes. Primary antibodies specific for mouse LAMP-1 (clone 1D4B), human LAMP-1 (clone H4A3) or mouse early endosomal antigen-1 (EEA1) were diluted in blocking buffer and incubated with cells at room temperature for 2 hours. For staining of microtubule networks, cells were fixed with methanol at -20°C for 3 minutes. Following fixation, cells were incubated with blocking buffer (PBS, 0.1% Tween 20, 5% serum) at room temperature for 30 minutes. The primary antibody specific for beta-tubulin was diluted in blocking buffer and incubated with cells at room temperature for 2 hours. After incubation with the primary antibodies, cells were washed with PBST (PBS, 0.1% Tween 20) and incubated

Author Manuscript Published OnlineFirst on September 22, 2017; DOI: 10.1158/1535-7163.MCT-17-0092
Author manuscripts have been peer reviewed and accepted for publication but have not yet been edited.

with fluorescently-labeled secondary antibodies diluted in blocking buffer for 1 hour at room temperature. To detect internalized PS agents, fluorescently-labeled goat or donkey anti-human IgG (H+L) antibody was used. Following incubation, cells were washed with PBST and mounted with ProLong Gold antifade mountant (Life Technologies, catalog # P36930).

Fluorescent images were acquired using a Zeiss Axiovert 200M inverted fluorescence microscope with a 63X, 1.4 NA plan apochromat objective (Carl Zeiss) and a 1.6X internal optovar. Fluorescent filter sets for GFP and Alexa 555 (Chroma Technology, catalog # 41017 and 41002b) were used for image acquisition. The acquired data were processed using the microscopy image analysis tool (MIATool) software (www4.utsouthwestern.edu/wardlab/miatool.asp).

PS pull-down assay

To study the Ca^{2+}-dependence of binding of the PS-specific Fc fusions to PS, proteins (100 nM) were diluted in binding buffer (10 mM HEPES pH 7.4, 150 mM NaCl with 2 mM or 2 μM Ca^{2+}). 50 μl PS-coated beads (Echelon, catalog # P-B0PS) were added and incubated at room temperature for 2 hours. The beads were then washed with the binding buffer and bound proteins detected by immunoblotting with HRP-conjugated goat anti-human IgG (H+L) antibody. To examine the pH-dependent binding to PS, proteins were diluted at 100 nM in PBS pH 7.4 or 6.0. 50 μl (bed volume) PS-coated beads were added, incubated at room temperature for 2 hours and samples processed as above.

Annexin V binding assay

One million cells were suspended in Annexin V binding solution (10 mM HEPES pH 7.4, 150 mM NaCl, 2.5 mM $CaCl_2$). Annexin V conjugated with Alexa 488 (Life Technologies, catalog #

A13201) was added to the cell suspension at a 1:100 dilution and incubated with the cells for 10 minutes at room temperature. Cells were then washed once with Annexin V binding solution and analyzed by flow cytometry (BD FACSCalibur). Flow cytometry data were processed using FlowJo (FLOWJO, LLC).

Flow cytometry analyses of PS-targeting agents

Cells were trypsinized and resuspended in flow cytometry buffer (PBS with Ca^{2+}/ Mg^{2+}, 1% BSA). 50 nM PS-specific Fc fusions were incubated with the cells for 30 minutes at either room temperature or on ice depending on the assay. Cells were washed with flow cytometry buffer and incubated with fluorophore-conjugated secondary antibodies on ice for 30 minutes. Cells were then washed and analyzed by flow cytometry (BD FACSCalibur). Flow cytometry data were processed using FlowJo (FLOWJO LLC).

Protein conjugation with maleimidocaproyl-val-cit-PAB-MMAE

20 μM Fc fusion or control antibody in PBS was incubated with 320 μM TCEP at room temperature for 3 hours to reduce the hinge disulfide bonds. Maleimidocaproyl-val-cit-PAB-MMAE (MC-VC-PAB-MMAE; Levena Biopharma, catalog # SET0201) was then added to the reduced Fc fusion or control antibody at a concentration of 160 μM and incubated at room temperature for 3 hours. Following the conjugation reaction, free MMAE was removed by dialysis of the protein against PBS. The conjugated Fc fusion or control antibody was stored at 4°C.

Cell growth and survival assays

Cells were plated into 96-well plates as follows: 2H11, 10,000 cells/well; MCF-7, SK-BR-3 and LNCaP, 5,000 cells/well; MDA-MB-231, 3,000 cells/well; 22Rv1, 15,000 cells/well. Cells were

grown overnight followed by the addition of PS-specific PDCs. Cell growth and survival were measured after 3-5 days incubation with the Cell Proliferation AQ One Solution Cell Proliferation Assay kit (Promega, catalog # G3581). Dose-response curves were plotted and IC_{50} values determined using GraphPad Prism software.

Pharmacokinetic and whole body imaging studies

Animal procedures used in all mouse studies were approved by the Institutional Animal Care and Use Committee of the University of Texas Southwestern Medical Center and Texas A&M University. All BALB/c SCID mice used in the study were purchased from The Jackson Laboratory (stock # 001803) and bred in-house. Pharmacokinetic studies were performed as described previously (20). Briefly, Lugol solution was added to drinking water 96 hours before the experiments. SCID BALB/c female mice (8 weeks old; 18-22 g weight) were anesthetized using 2% isoflurane in oxygen and injected (i.v.) with ^{125}I-labeled proteins (100-120 µCi, 10-12 µg/mouse) in 200 µl PBS with 0.1% BSA. Whole body radioactive counts were measured using a Biodex Atomlab 100 dose calibrator. Blood radioactive counts were measured by retro-orbitally bleeding mice with 10 µl capillary tubes (Drummond) and radioactive counts (cpm) determined by gamma counting (Perkin Elmer).

For whole body, near infrared imaging (NIR), female nude mice (6-7 weeks old; purchased from Envigo, catalog # 6903F) or BALB/c SCID mice (6-8 weeks old) were used. For implantation of MDA-MB-231 tumors, mice were anesthetized with 2% isoflurane in oxygen and a small surgical incision was made to expose the mammary fat pad. MDA-MB-231 cells were trypsinized and dispersed into single cell suspensions in PBS. 5 x 10^6 cells/mouse were injected in 100 µl into the mammary fat pad, using a 25G needle, and the incision was then sealed with a wound clip. Buprenorphine was administered (s.c.) at 50 µg/kg immediately following the surgery and 12 hours later. Mice were monitored daily and the wound clip was removed one week post-surgery.

Author Manuscript Published OnlineFirst on September 22, 2017; DOI: 10.1158/1535-7163.MCT-17-0092
Author manuscripts have been peer reviewed and accepted for publication but have not yet been edited.

For imaging of nude mice, mice were divided into 3 groups (n = 3 mice per group) when tumors reached sizes of approximately 150 mm^3 and administered (i.p.) with 5 mg/Kg docetaxel 72 and 48 hours before being injected (i.v.) with 1 nmole IRDye800CW-labeled PS-specific agents in PBS. Fluorescence imaging (FLI) was performed using a Caliper Xenogen IVIS Spectrum (Perkin Elmer) *in vivo* imaging system at 0 (before injection) and 3, 24 and 48 hours post-injection. FLI was performed using 745 nm excitation, 800 nm emission, binning 8, FOV 12.9 cm, f-stop 2 and auto-exposure. Data were quantitated with the Living Imaging software using absolute Radiant Efficiency (photons/s) in an ROI, manually drawn to outline the FLI signal of the tumor and normalized to the tumor volumes.

For analyses of tumor localization in BALB/c SCID mice, mice were divided into 3 groups (n = 3 mice per group) when tumors reached sizes of approximately 300 mm^3 and administered (i.p.) with 5 mg/Kg docetaxel 72 and 48 hours before being injected (i.v.) with 1 nmole of IRDye800CW-labeled PS-specific agents in PBS. 48 hours following injection, tumors were dissected out and imaged as above. Fluorescence in an ROI, manually drawn to outline the FLI signal of the tumor, was quantitated and normalized to the tumor weight.

Mouse xenograft studies

Implantation of MDA-MBA-231 tumor xenografts in BALB/c SCID mice was carried out as described for the whole body imaging experiments. For implantation of LNCaP tumors, 7-8 week old male BALB/c SCID mice (18-22 g weight) were anesthetized with 2% isoflurane in oxygen and 5 x 10^6 LNCaP cells suspended in 50% RPMI and 50% Matrigel (BD Biosciences) were injected (s.c.). When MDA-MBA-231 or LNCaP tumors reached a size of ~100 mm^3, mice were injected (i.p.) with 5 mg/Kg docetaxel 72 and 48 hours before the treatment. Mice were then injected (i.v.) with 1 nmole unconjugated proteins, PDCs or PBS vehicle as indicated in the figure legends twice per week. Tumors and body weights were measured twice a week. For the

treatment experiment using Fc-Syt1(DN)_MMAE, mice were treated for 4 weeks and monitored for another 2.5 weeks. Experiments were terminated when the tumor size reached 2 cm in any dimension.

Immunohistochemical analyses

Female BALB/c SCID mice bearing MDA-MB-231 tumors were treated (i.p.) with 5 mg/Kg docetaxel 72 and 48 hours before i.v. delivery of either PBS vehicle or 1 nmole Fc-Syt1 conjugated with MMAE. At different time points, mice were perfused (i.c.) with PBS followed by 4% PFA. Tumors were then dissected out, embedded in OCT (Fisher Scientific, catalog # 23-730-571) and stored at -80°C. 10 µm tissue sections were cut and hydrated with PBS at room temperature before fixation with 4% PFA for 30 minutes. Tumor sections were then washed with PBS and incubated with the permeabilization / blocking solution (PBS, 0.5% Triton X-100, 3% BSA) at room temperature for 1 hour. Primary antibodies for human Ki-67, mouse CD31 and F4/80 were diluted in the blocking buffer (PBS, 0.1% Tween 20, 5% serum) and incubated with the tissue sections at 4°C overnight. The next day, tissue sections were washed with PBST (PBS, 0.1% Tween 20) and incubated with the fluorophore-conjugated secondary antibodies diluted in the blocking buffer at room temperature for 2 hours. After washing with PBST, tissue sections were mounted with ProLong Gold antifade mounting medium. Confocal images were acquired using a Nikon A1R confocal microscope equipped with the 40X, 1.3 NA plan fluor objective and processed with the NIS-Elements software (Nikon).

Results

Generation and characterization of PS-targeting agents

A panel of PS-targeting agents was generated by fusing the Fc region of human IgG1 to the following PS-binding domains: core domain of Annexin A1 (AnxA1), C2A domain of Synaptotagmin 1 (Syt1) and C2 domain of PKCα (Fig. 1A). The three domains bind to PS in a Ca^{2+}-dependent manner (4,27,28) and the resulting fusion proteins were designated Fc-AnxA1, Fc-Syt1 and Fc-PKCα, respectively. The PS-targeting agents were expressed and purified as homodimers (Fig. 1A and Supplementary Fig. S1) and bound to PS in a lipid binding assay (Fig. 1B). They also bound to cardiolipin, which is located on the inner mitochondrial membrane of eukaryotic cells and therefore not relevant to targeting. By contrast with Fc-Syt1 and Fc-PKCα, Fc-AnxA1 exhibited a broader lipid binding profile and bound both neutral and negatively-charged lipids (Fig. 1B). Importantly, none of the PS-binding agents bound phosphatidylcholine (PC) and sphingomyelin, lipids that are present in the plasma membrane outer leaflet.

The tumor endothelial cell line 2H11 (29) and triple negative breast tumor cell line MDA-MB-231 were used to investigate the ability of the PS-binding agents to interact with lipids on the cell surface. Binding of fluorescent Annexin V showed that both of these cell lines expose PS and that PS exposure increases following docetaxel treatment (Supplementary Fig. S2). All PS-binding agents interacted with PS-positive cells, with Fc-Syt1 showing lower levels of binding than Fc-AnxA1 and Fc-PKCα (Fig. 1C).

To determine which recombinant proteins were suitable for further development as protein-drug conjugates (PDCs), we evaluated the pharmacokinetic behavior and tumor localization of the three PS-binding agents in mice. Pharmacokinetic studies of the PS-binding agents revealed that Fc-Syt1 persisted at both the whole body and blood levels for significantly longer than the

other two proteins (Fig. 1D and E). Binding analyses demonstrated that these three fusion proteins had similar affinities for binding to recombinant mouse FcRn at pH 6.0, with no detectable binding or affinity too low to accurately determine at pH 7.4 (Table 1), indicating that affinity differences do not contribute to the longer persistence of Fc-Syt1. The proteins were labeled with the residualizing dye, IRDye800CW, and injected (i.v.) into female nude mice bearing MDA-MB-231 xenografts and imaged at different time points (Fig. 1F) with tumor fluorescence quantitated 48 hours post-injection (Fig. 1G). Similar experiments were carried out in BALB/c SCID mice and 48 hours later, tumors were excised and dye levels determined (Fig. 1H and I). Amongst the three PS-specific agents, Fc-Syt1 exhibited the highest level of tumor localization. Collectively, these results indicated that of the three PS-targeting agents, Fc-Syt1 is the most promising for conversion to a PDC for use in therapy.

Cell binding and internalization of bivalent and tetravalent PS-specific Fc-fusions

For therapeutic efficacy of antibody-drug conjugates (ADCs), target cell internalization of the ADC and release of the toxic payload in late endosomes or lysosomes is essential (11). In several receptor systems it has been shown that multivalent ligands, or mixtures of cross-linking ligands such as antibodies, promote receptor internalization and degradation (30-32). To study the role of avidity in the behavior of PS-targeting PDCs, we also generated tetravalent Syt1-Fc-Syt1 that contains four Syt1 C2A domains (Fig. 2A). The tetravalent protein was purified as a homodimer (Fig. 2A and Supplementary Fig. S3A). As designed, Syt1-Fc-Syt1 has higher affinity/avidity for PS than Fc-Syt1 in lipid binding assays (Fig. 2B) and the same lipid selectivity as its bivalent parent, Fc-Syt1 (Fig. 2C). Consistent with the binding data shown in Fig. 2B, the tetravalent Syt1-Fc-Syt1 bound to 2H11 cells at significantly higher levels than bivalent Fc-Syt1 protein (Fig. 2D).

Author Manuscript Published OnlineFirst on September 22, 2017; DOI: 10.1158/1535-7163.MCT-17-0092
Author manuscripts have been peer reviewed and accepted for publication but have not yet been edited.

We next compared the internalization of Fc-Syt1 and Syt1-Fc-Syt1 using Alexa 647-labeled proteins. 2H11 cells were incubated with labeled Fc-Syt1 and Syt1-Fc-Syt1 on ice at different concentrations to achieve similar surface binding followed by incubation at 37°C to allow internalization for different times. Surface-bound proteins were stripped off with EDTA (due to the Ca^{2+} dependence of binding) and internalized levels (resistant to stripping) were determined by flow cytometry. These studies indicated that although both proteins efficiently accumulated within cells, the tetravalent Syt1-Fc-Syt1 was internalized more rapidly compared with bivalent Fc-Syt1 (Fig. 2E). Fluorescent microscopy was also used to study the subcellular trafficking behavior of the Syt1-Fc fusion proteins. In both 2H11 and MDA-MB-231 cells, Fc-Syt1 and Syt1-Fc-Syt1 were internalized and delivered into LAMP-1 positive lysosomes (Fig. 2F, G and Supplementary Fig. S3B).

Calcium sensing and endosomal release of PS-specific PDCs

The lysosomal trafficking and internalization behavior of Fc-Syt1 and Syt1-Fc-Syt1 indicated that they could be effective as delivery vehicles for conjugated drugs. We therefore conjugated maleimidocaproyl-val-cit-PAB-MMAE (33) to hinge cysteines (Fig. 3A, left panel). For use as a negative control, MMAE was conjugated to a hen egg lysozyme-specific human IgG1 (21) in which the light/heavy chain-interacting cysteine residues were mutated to serine to result in four possible conjugation sites. SDS-PAGE analyses indicated that the conjugations had gone to completion and resulted in drug to antibody ratios (DARs) of four (Fig. 3A, right panel). The DARs of four for both MMAE-conjugated Fc-Syt1 and Syt1-Fc-Syt1 were confirmed by MALDI-TOF mass spectrometry. Since complete conjugation disrupted the two disulfide bonds in the hinge region, apparent molecular weights of 43.6 kDa for Fc-Syt1_MMAE and 58.6 kDa for Syt1-Fc-Syt1_MMAE, respectively, were observed in these analyses (Supplementary Fig. S4A and S4B, upper panels). This contrasted with the unconjugated or partially conjugated protein

that retained two or one disulfide bonds respectively, resulting in an apparent molecular weight of approximately 82 kDa for Fc-Syt1 and 112 kDa for Syt1-Fc-Syt1 (Supplementary Fig. S4A and S4B, lower panels). Importantly, the conjugation process did not lead to protein aggregation (Supplementary Fig. S4C).

The Syt1 C2A domain requires Ca^{2+} for PS binding (23). The lower Ca^{2+} concentration in early/sorting endosomes (~2 μM) compared with the extracellular Ca^{2+} levels (1 - 2 mM) suggests that following internalization, PS-specific PDCs will dissociate from the limiting membrane of these endosomes (18,19). This dissociation is expected to lead to improved lysosomal delivery. Both PS-specific PDCs containing Syt1 domains bound to PS-beads in buffer containing 2 mM Ca^{2+}, but no detectable interaction was observed when the Ca^{2+} concentration was decreased to 2 μM (Fig. 3B, left panel). In addition, because the pH within sorting (early) endosomes is acidic (pH 6.0-6.5) (34), we analyzed the effect of pH on PDC:PS interactions. Both PDCs bound to PS at similar levels in the pH range 6.0-7.4 (Fig. 3B, right panel). Consistent with the *in vitro* binding analyses demonstrating Ca^{2+}-dependent binding, fluorescence microscopy analyses showed the presence of the PS-specific PDCs in the lumen, rather than limiting membrane of sorting endosomes in MDA-MB-231 cells following 15 and 30 minutes co-incubation with PDC (Fig. 3C and Supplementary Fig. S5A). The relatively large size (~1.5 μm diameter) of the sorting endosomes in MDA-MB-231 cells, which was also observed with untreated cells (Supplementary Fig. S5B), enabled PDC dissociation from the limiting endosomal membrane to be quantitated (Fig. 3C, right panels). Fc-Syt1_MMAE and Syt1-Fc-Syt1_MMAE could be detected in lysosomes within 30 minutes and the level of Fc fusion increased following four hours of co-incubation (Fig. 3D and Supplementary Fig. S5C). In addition, both PDCs disrupted the microtubular network in 2H11 and MDA-MB-231 cells (Fig. 3E and F).

Inhibition of growth and survival of PS-positive cells by PS-specific PDCs

We examined the effects of PS-specific PDCs on the growth of multiple cell lines, including tumor endothelium (2H11), ER positive breast cancer (T-47D), HER2-positive breast cancer (SK-BR-3), triple negative breast cancer (MDA-MB-231), androgen sensitive prostate cancer (LNCaP) and castration resistant prostate cancer (22Rv1). Staining of the cells with fluorescently labeled Annexin V showed that all of these cell lines were PS-positive (Supplementary Fig. S6A). Incubation of PS-ADCs effectively inhibited the growth and survival of the cells in a dose-dependent manner (Fig. 4 and Table 2). Although the tetravalent Syt1-Fc-Syt1_MMAE was more potent in inhibiting T-47D cell growth than the bivalent Fc-Syt1_MMAE, the two PDCs exhibited similar effects on the other cell lines. Consistent with the growth inhibitory effects, the internalization of the two PDCs at concentrations close to the corresponding IC_{50}s were similar for all cell lines, except that Syt1-Fc-Syt1_MMAE was internalized at higher levels than Fc-Syt1_MMAE for T-47D cells (Supplementary Fig. S6B). Relatively high concentrations of the control IgG (hen egg lysozyme-specific human IgG1) conjugated with MMAE resulted in inhibition of cell growth, possibly due to nonspecific fluid phase uptake of the drug, whereas unconjugated PS-targeting proteins showed no effect on cell growth (Supplementary Fig. S6C). Thus, our data indicate that Syt1-based PDCs are potent inhibitors of tumor endothelial and cancer cell growth *in vitro*.

Inhibition of tumor growth by PS-specific PDCs in mouse xenograft models

We next investigated the therapeutic effects of the PS-specific PDCs against tumor xenografts in SCID mice. Prior to therapy, pharmacokinetic studies of the PS-specific PDCs demonstrated that tetravalent Syt1-Fc-Syt1_MMAE had a shorter half-life than bivalent Fc-Syt1_MMAE (Fig. 5A and B), possibly due to increased target-mediated uptake. Due to the relatively short half-lives, we delivered the PDCs (1 nmole/mouse) into tumor-bearing mice twice per week. In

female SCID mice bearing orthotopic MDA-MB-231 breast tumors that had been pretreated with docetaxel, bivalent Fc-Syt1_MMAE potently blocked breast tumor growth (Fig. 5C). Tetravalent Syt1-Fc-Syt1_MMAE also inhibited tumor growth, but was less effective than bivalent Fc-Syt1_MMAE. Treatment with unconjugated Fc-Syt1 and Syt1-Fc-Syt1 had no effect on tumor growth (Fig. 5C).

In addition to efficacy in the breast tumor model, bivalent Fc-Syt1_MMAE completely blocked tumor growth in male SCID mice bearing prostate cancer LNCaP xenografts that had been pretreated with docetaxel. Consistent with the *in vitro* data (Supplementary Fig. S6C), the unconjugated protein had no effect (Fig. 5D). However, tetravalent Syt1-Fc-Syt1_MMAE did not significantly inhibit tumor growth. The most likely explanation for this difference is the shorter *in vivo* persistence of the tetravalent PDC. Taken together with the breast tumor data, these results indicate that the valency of the PS-specific PDCs has a profound influence on their therapeutic outcomes. Importantly, we did not observe weakness or loss of body weight in any of the treatment groups (Fig. 5E and Supplementary Fig. S7), indicating that PS-specific PDCs are well-tolerated *in vivo*.

To further validate that Fc-Syt1_MMAE binds PS-positive cells in tumor tissue following docetaxel treatment, we performed immunohistochemistry following delivery of this PDC into tumor-bearing mice. We found that Fc-Syt1_MMAE was localized to CD31-positive blood vessels (Fig. 5F), tumor cells and tumor-infiltrating F4/80-positive macrophages (Fig. 5G) which can expose PS (5). The data indicates that cancer cells not only expose PS *in vitro* (Supplementary Fig. S6A) (3,35), but retain this loss of PS asymmetry *in vivo*.

Inhibition of tumor growth by Fc-Syt1_MMAE is dependent on PS-binding

To exclude the possibility that the drug accumulated in the tumor through non-specific mechanisms such as the enhanced permeability and retention (EPR) effect (36) and to show that the *in vivo* efficacy was dependent on PS binding, we generated a mutated variant of the synaptotagmin 1 C2A domain with decreased affinity for PS. The C2A domain of synaptotagmin 1 interacts with PS through three Ca^{2+} ions chelated by five aspartic acids (D) in domain loops I and III (23). To ablate Ca^{2+} binding, we mutated all five aspartic acid residues to asparagines (N) to produce Fc-Syt1(DN). Fc-Syt1(DN) was purified as a homodimer and interacted with PS at essentially background levels in the protein-lipid overlay assay (Fig. 6A and B). Moreover, Fc-Syt1(DN) had significantly reduced binding to PS-positive cells compared with its wild-type counterpart (Fig. 6C). This mutated protein and as a control, human IgG1-derived Fc, were conjugated to MMAE and analyzed using mass spectrometry. These analyses indicated conjugation ratios of four drugs per protein molecule (Supplementary Fig. S8A and S8B). In addition, size exclusion analyses demonstrated that the resulting MMAE-conjugated proteins were not aggregated (Supplementary Fig. S8C). Mice bearing orthotopic MDA-MB-231 tumors were pretreated with docetaxel prior to treatment with PDCs (1 nmole/mouse) or vehicle control for four weeks, until mice in the control (PBS) group were euthanized due to their large tumor sizes. Treatment of MDA-MB-231 tumors with Fc-Syt1_MMAE led to potent growth inhibition (Fig. 6D). More importantly, tumor growth remained inhibited after the treatment with Fc-Syt1_MMAE was stopped at four weeks. No tumors could be isolated from three of six mice at the end of the experiment (Fig. 6E). Although the delivery of Fc_MMAE or Fc-Syt1(DN)_MMAE slowed tumor growth initially, rapid proliferation was observed following the end of treatment (Fig. 6D). Collectively, the data indicate that PS-binding is essential for the activity of Fc-Syt1_MMAE.

Discussion

ADCs represent a rapidly expanding class of therapeutics to target cancer. For the majority of ADC or PDC platforms, therapeutic efficacy is dependent on internalization and trafficking of the cytotoxic drug to lysosomes (11,12). The current study describes a novel approach for the generation of a PDC to its target, namely exposed PS on tumor cells and tumor vascular endothelium. First, we have identified a PS-targeting protein that is efficiently internalized into cells that expose PS. Second, we have exploited the Ca^{2+}-dependence of the PS-Syt1 interaction to enable endosomal dissociation, and consequent lysosomal delivery, of the Syt1-based PDC. Third, we have tuned the binding strength of the PS-targeting agent to optimize pharmacokinetic behavior and delivery to the tumor site. We demonstrate that the resulting PDC, Fc-Syt1_MMAE, has potent anti-tumor effects in mouse models of breast and prostate cancer.

Amongst the three PS-targeting agents developed here, both Fc-AnxA1 and Fc-PKCα exhibited higher levels of binding to target cells than Fc-Syt1. However, of these three agents, Fc-Syt1 exhibited the highest tumor accumulation in mice. The data indicate that high affinity interactions with PS negatively impact the *in vivo* behavior with respect to tumor localization. There are two possible reasons for this behavior: First, PS exposure has also been identified in non-apoptotic normal cells such as differentiating monocytes and a subpopulation of T cells (16,17). Although the SCID mice used in the current study lack T cells, monocytes may therefore act as a sink for target-mediated clearance outside the tumor tissue. This sink effect is expected to be greater for higher affinity PS-specific agents, resulting in shorter *in vivo* persistence. Consistent with this, pharmacokinetic studies demonstrate that Fc-Syt1 has a significantly longer half-life compared with Fc-AnxA1 and Fc-PKCα. Further, bivalent Fc-Syt1_MMAE also displayed a longer half-life and better *in vivo* efficacy than higher avidity, tetravalent Syt1-Fc-Syt1_MMAE. Second, besides the influence on *in vivo* persistence, higher affinity HER2-specific antibodies have been shown

to penetrate tumors less efficiently than their lower affinity counterparts (the “binding barrier theory” (37-39)). Similar pathways may operate during PS-targeting.

Interestingly, our study showed Fc-Syt1_MMAE could potently inhibit tumor growth in mice, whereas unconjugated Fc-Syt1 had no effect. This contrasts with bavituximab, which has been reported to be therapeutically effective as an unconjugated antibody in pre-clinical models when combined with radiation, chemotherapy or other procedures that increase PS exposure in tumor tissues (6-10). One possible reason for this difference is that we delivered the chemotherapeutic drug, docetaxel, as two doses at the beginning of the treatment to elevate tumor PS exposure, whereas in the bavituximab study, mice were treated in combination with antibody and docetaxel throughout therapy. The importance of increasing PS exposure using either chemotherapy or radiation for tumor localization of PS-targeting agents was indicated by a recent study in which two antibodies with β2GP1-independent specificity for PS, PA and cardiolipin failed to accumulate in tumor-bearing mice that were not treated with docetaxel or other ‘PS-inducing’ agents (40).

The induction of endosomal dissociation of antibodies from their target antigen, by exploiting the lower pH or Ca^{2+} concentration within early/sorting endosomes relative to the extracellular environment, has been described by us and others as a strategy to clear antigens such as inflammatory cytokines or their soluble, signaling competent receptors (41-43). This release of target is followed by recycling and exocytosis of the antibody through binding to the Fc receptor, FcRn, which is expressed in most normal parenchymal and hematopoietic cells (20,44,45). To date, this approach has been implemented by using antibody engineering to generate antibodies that bind with pH-dependence or Ca^{2+}-dependence (41-43). Here we use naturally occurring proteins that have intrinsic Ca^{2+}-dependence for binding to target, thereby avoiding the need for engineering. Recent data including our own indicate that, in general, tumor cells

express very low or undetectable levels of the recycling receptor, FcRn (46,47). This loss of expression is critical for efficacy of Ca^{2+}-switched ADCs/PDCs, since it avoids the possibility of FcRn-mediated salvage of the drug-conjugate away from lysosomal delivery following endosomal dissociation from target.

To summarize, we have developed a novel PDC that dissociates from target in early endosomes through Ca^{2+}-switching, enabling lysosomal delivery of the drug regardless of ligand (PS) trafficking. Our study also reveals a complex relationship between *in vivo* efficacy of the PS-targeting agent and *in vitro* binding properties, with the lowest affinity PDC, Fc-Syt1_MMAE, showing superior pharmacokinetic properties and potent anti-tumor effects. Given that the subcellular trafficking behavior of many tumor surface markers following endosomal delivery remains poorly characterized, and most solid tumor antigens are not exclusively tumor-specific, our study indicates that approaches involving Ca^{2+}-switching and affinity/avidity tuning may have value for the design of effective ADC or PDC platforms.

Acknowledgements

This study is dedicated to the memory of our colleague, Philip Thorpe. We thank Alex Winters and Jeni Gerberich for assistance with the whole body imaging experiments, Jacob Newman for assistance with the construction of expression plasmids for the PS-specific Fc fusions and Drs. Dilip Challa and Priyanka Khare for providing recombinant mouse FcRn.

References

1. Connor J, Bucana C, Fidler IJ, Schroit AJ. Differentiation-dependent expression of phosphatidylserine in mammalian plasma membranes: quantitative assessment of outer-leaflet lipid by prothrombinase complex formation. Proc Natl Acad Sci U S A 1989;86:3184-8

2. Ran S, Downes A, Thorpe PE. Increased exposure of anionic phospholipids on the surface of tumor blood vessels. Cancer Res 2002;62:6132-40

3. Riedl S, Rinner B, Asslaber M, Schaider H, Walzer S, Novak A, et al. In search of a novel target - phosphatidylserine exposed by non-apoptotic tumor cells and metastases of malignancies with poor treatment efficacy. Biochim Biophys Acta 2011;1808:2638-45

4. Leventis PA, Grinstein S. The distribution and function of phosphatidylserine in cellular membranes. Annu Rev Biophys 2010;39:407-27

5. DeRose P, Thorpe PE, Gerber DE. Development of bavituximab, a vascular targeting agent with immune-modulating properties, for lung cancer treatment. Immunotherapy 2011;3:933-44

6. He J, Yin Y, Luster TA, Watkins L, Thorpe PE. Antiphosphatidylserine antibody combined with irradiation damages tumor blood vessels and induces tumor immunity in a rat model of glioblastoma. Clin Cancer Res 2009;15:6871-80

7. Yin Y, Huang X, Lynn KD, Thorpe PE. Phosphatidylserine-targeting antibody induces M1 macrophage polarization and promotes myeloid-derived suppressor cell differentiation. Cancer Immunol Res 2013;1:256-68

8. Huang X, Bennett M, Thorpe PE. A monoclonal antibody that binds anionic phospholipids on tumor blood vessels enhances the antitumor effect of docetaxel on human breast tumors in mice. Cancer Res 2005;65:4408-16

9. Cheng X, Li L, Thorpe PE, Yopp AC, Brekken RA, Huang X. Antibody-mediated blockade of phosphatidylserine enhances the antitumor effect of sorafenib in hepatocellular carcinomas xenografts. Ann Surg Oncol 2016; 23:583-591.

10. Beck AW, Luster TA, Miller AF, Holloway SE, Conner CR, Barnett CC, et al. Combination of a monoclonal anti-phosphatidylserine antibody with gemcitabine strongly inhibits the growth and metastasis of orthotopic pancreatic tumors in mice. Int J Cancer 2006;118:2639-43

11. Sievers EL, Senter PD. Antibody-drug conjugates in cancer therapy. Annu Rev Med 2013;64:15-29

12. Goldmacher VS, Kovtun YV. Antibody-drug conjugates: using monoclonal antibodies for delivery of cytotoxic payloads to cancer cells. Ther Deliv 2011;2:397-416

13. Bakhtiar R. Antibody drug conjugates. Biotechnol Lett 2016;38:1655-64

14. Chari RV, Miller ML, Widdison WC. Antibody-drug conjugates: an emerging concept in cancer therapy. Angew Chem Int Ed Engl 2014;53:3796-827

15. Kenis H, Reutelingsperger C. Targeting phosphatidylserine in anti-cancer therapy. Curr Pharm Des 2009;15:2719-23

16. Elliott JI, Surprenant A, Marelli-Berg FM, Cooper JC, Cassady-Cain RL, Wooding C, et al. Membrane phosphatidylserine distribution as a non-apoptotic signalling mechanism in lymphocytes. Nat Cell Biol 2005;7:808-16

17. Callahan MK, Halleck MS, Krahling S, Henderson AJ, Williamson P, Schlegel RA. Phosphatidylserine expression and phagocytosis of apoptotic thymocytes during differentiation of monocytic cells. J Leukoc Biol 2003;74:846-56

18. Albrecht T, Zhao Y, Nguyen TH, Campbell RE, Johnson JD. Fluorescent biosensors illuminate calcium levels within defined beta-cell endosome subpopulations. Cell Calcium 2015;57:263-74

19. Gerasimenko JV, Tepikin AV, Petersen OH, Gerasimenko OV. Calcium uptake via endocytosis with rapid release from acidifying endosomes. Curr Biol 1998;8:1335-8

20. Montoyo HP, Vaccaro C, Hafner M, Ober RJ, Mueller W, Ward ES. Conditional deletion of the MHC class I-related receptor FcRn reveals the sites of IgG homeostasis in mice. Proc Natl Acad Sci U S A 2009;106:2788-93

21. Foote J, Winter G. Antibody framework residues affecting the conformation of the hypervariable loops. J Mol Biol 1992;224:487-99

22. Neuberger MS. Expression and regulation of immunoglobulin heavy chain gene transfected into lymphoid cells. EMBO J 1983;2:1373-8

23. Striegel AR, Biela LM, Evans CS, Wang Z, Delehoy JB, Sutton RB, et al. Calcium binding by synaptotagmin's C2A domain is an essential element of the electrostatic switch that triggers synchronous synaptic transmission. J Neurosci 2012;32:1253-60

24. Popov S, Hubbard JG, Kim J, Ober B, Ghetie V, Ward ES. The stoichiometry and affinity of the interaction of murine Fc fragments with the MHC class I-related receptor, FcRn. Mol Immunol 1996;33:521-30

25. Ober RJ, Ward ES. Compensation for loss of ligand activity in surface plasmon resonance experiments. Anal Biochem 2002;306:228-36

26. Zhou J, Mateos F, Ober RJ, Ward ES. Conferring the binding properties of the mouse MHC class I-related receptor, FcRn, onto the human ortholog by sequential rounds of site-directed mutagenesis. J Mol Biol 2005;345:1071-81

27. Schutters K, Reutelingsperger C. Phosphatidylserine targeting for diagnosis and treatment of human diseases. Apoptosis 2010;15:1072-82

28. Gerke V, Creutz CE, Moss SE. Annexins: linking Ca2+ signalling to membrane dynamics. Nat Rev Mol Cell Biol 2005;6:449-61

29. Walter-Yohrling J, Morgenbesser S, Rouleau C, Bagley R, Callahan M, Weber W, et al. Murine endothelial cell lines as models of tumor endothelial cells. Clin Cancer Res 2004;10:2179-89

30. Friedman LM, Rinon A, Schechter B, Lyass L, Lavi S, Bacus SS, et al. Synergistic down-regulation of receptor tyrosine kinases by combinations of mAbs: implications for cancer immunotherapy. Proc Natl Acad Sci U S A 2005;102:1915-20

31. Spangler JB, Neil JR, Abramovitch S, Yarden Y, White FM, Lauffenburger DA, et al. Combination antibody treatment down-regulates epidermal growth factor receptor by inhibiting endosomal recycling. Proc Natl Acad Sci U S A 2010;107:13252-7

32. Kang JC, Poovassery JS, Bansal P, You S, Manjarres IM, Ober RJ, et al. Engineering multivalent antibodies to target heregulin-induced HER3 signaling in breast cancer cells. MAbs 2014;6:340-53

33. Doronina SO, Toki BE, Torgov MY, Mendelsohn BA, Cerveny CG, Chace DF, et al. Development of potent monoclonal antibody auristatin conjugates for cancer therapy. Nat Biotechnol 2003;21:778-84

34. Casey JR, Grinstein S, Orlowski J. Sensors and regulators of intracellular pH. Nat Rev Mol Cell Biol 2010;11:50-61

35. Vallabhapurapu SD, Blanco VM, Sulaiman MK, Vallabhapurapu SL, Chu Z, Franco RS, et al. Variation in human cancer cell external phosphatidylserine is regulated by flippase activity and intracellular calcium. Oncotarget 2015;6:34375-88

36. Matsumura Y, Maeda H. A new concept for macromolecular therapeutics in cancer chemotherapy: mechanism of tumoritropic accumulation of proteins and the antitumor agent smancs. Cancer Res 1986;46:6387-92

37. Rudnick SI, Lou J, Shaller CC, Tang Y, Klein-Szanto AJ, Weiner LM, et al. Influence of affinity and antigen internalization on the uptake and penetration of Anti-HER2 antibodies in solid tumors. Cancer Res 2011;71:2250-9

38. Thurber GM, Schmidt MM, Wittrup KD. Antibody tumor penetration: transport opposed by systemic and antigen-mediated clearance. Adv Drug Deliv Rev 2008;60:1421-34

39. Adams GP, Schier R, McCall AM, Simmons HH, Horak EM, Alpaugh RK, et al. High affinity restricts the localization and tumor penetration of single-chain Fv antibody molecules. Cancer Res 2001;61:4750-5

40. Bujak E, Pretto F, Neri D. Generation and tumor recognition properties of two human monoclonal antibodies specific to cell surface anionic phospholipids. Invest New Drugs 2015;33:791-800

41. Igawa T, Ishii S, Tachibana T, Maeda A, Higuchi Y, Shimaoka S, et al. Antibody recycling by engineered pH-dependent antigen binding improves the duration of antigen neutralization. Nat Biotechnol 2010;28:1203-7

42. Hironiwa N, Ishii S, Kadono S, Iwayanagi Y, Mimoto F, Habu K, et al. Calcium-dependent antigen binding as a novel modality for antibody recycling by endosomal antigen dissociation. MAbs 2016;8:65-73

43. Devanaboyina SC, Lynch SM, Ober RJ, Ram S, Kim D, Puig-Canto A, et al. The effect of pH dependence of antibody-antigen interactions on subcellular trafficking dynamics. MAbs 2013;5:851-9

44. Zhu X, Meng G, Dickinson BL, Li X, Mizoguchi E, Miao L, et al. MHC class I-related neonatal Fc receptor for IgG is functionally expressed in monocytes, intestinal macrophages, and dendritic cells. J Immunol 2001;166:3266-76

45. Akilesh S, Christianson GJ, Roopenian DC, Shaw AS. Neonatal FcR expression in bone marrow-derived cells functions to protect serum IgG from catabolism. J Immunol 2007;179:4580-8

46. Swiercz R, Chiguru S, Tahmasbi A, Ramezani SM, Hao G, Challa DK, et al. Use of Fc-Engineered Antibodies as Clearing Agents to Increase Contrast During PET. J Nucl Med 2014;55:1204-7

47. Dalloneau E, Baroukh N, Mavridis K, Maillet A, Gueugnon F, Courty Y, et al. Downregulation of the neonatal Fc receptor expression in non-small cell lung cancer tissue is associated with a poor prognosis. Oncotarget 2016;7:54415-54429

Tables

Table 1. Equilibrium dissociation constants for the interactions of recombinant proteins with mouse FcRn at pH 6.0 and 7.4 determined using surface plasmon resonance.

Proteins	K_D (nM), pH 6.0	K_D (nM), pH 7.4
Human IgG1[1]	57.1	n.b.[2]
Fc	66.8	n.b.[2]
Fc-AnxA1	74.1	n.b.[2]
Fc-Syt1	69.4	n.b.[2]
Fc-PKCα	69.1	n.b.[2]

[1]human IgG1 is the hen egg lysozyme-specific antibody, HuLys10 (21); [2]n.b., no detectable binding, or affinity too low to accurately determine.

Table 2. IC_{50} values for PS-specific PDCs.

IC_{50} (nM)	2H11	T-47D	SK-BR-3	MDA-MB-231	LNCaP	22Rv1
Fc-Syt1_MMAE	7.0	14.1	1.2	9.1	7.6	6.0
Syt1-Fc-Syt1_MMAE	5.7	6.9	1.8	6.1	7.3	7.9

Figure Legends

Figure 1. Generation and characterization of PS-targeting agents. **A,** schematic representation of PS agents (left panel). Filled circles and rectangles represent the PS-binding domains and IgG1 hinge region, respectively. Right panel shows reducing SDS-PAGE analyses of the PS-specific Fc fusions, with molecular weights (MW) shown in kDa on the left. **B,** lipid binding profiles of PS-specific Fc fusions using lipid-coated nitrocellulose membranes. Bound proteins were detected with goat anti-human IgG (H+L) antibody conjugated with HRP. **C,** binding of PS-specific Fc fusions to PS-positive 2H11 and MDA-MB-231 cells using flow cytometry analysis, using Alexa 647-labeled anti-human IgG (H+L) for detection. 2^{nd} and Fc represent negative controls using secondary conjugate or recombinant Fc fragment, respectively. **D,** pharmacokinetic analyses of PS-specific Fc fusions in BALB/c SCID mice (n = 5 mice/group). Whole body and blood levels of radioactivity were measured at the indicated time points. **E,** areas under curves in panel **D** for whole body (upper panel) and blood (lower panel) counts were quantitated. **F,** nude mice bearing orthotopic human MDA-MB-231 tumors (n = 3 mice/group) were injected with IRDye800CW-labeled PS-specific Fc fusions, and NIR fluorescence images acquired at the indicated time points. **G,** tumor-associated fluorescence intensities at 48 hours in **F** normalized to the corresponding tumor volumes were quantitated. **H,** female BALB/c SCID mice bearing MDA-MB-231 tumors (n = 3 mice/group) were injected with IRDye800CW-labeled PS-specific agents. 48 hours post-injection, tumors were dissected out and NIR images were acquired. **I,** tumor-associated fluorescence intensities in **H** normalized to the corresponding tumor weights. Statistically significant differences in **E**, **G** and **I** were analyzed using one-way ANOVA followed by Tukey *post hoc* test (**, $P < 0.01$; ***, $P < 0.001$; ****, $P < 0.0001$). Error bars in **D**, **E**, **G** and **I** represent SEM.

Figure 2. Cell binding and internalization of PS-specific Fc fusions containing Syt1 C2A. **A,** schematic representation of bivalent and tetravalent PS-specific Fc fusions with filled circles representing the Syt1 C2A domain (left panel). Right panel shows reducing SDS-PAGE analyses of the Syt1-Fc fusions, with molecular weights (MW) shown in kDa on the right. **B,** Fc fusions (25 nM) were incubated with nitrocellulose membranes coated with the indicated amounts of PS. Bound proteins were detected with goat anti-human IgG (H+L) antibody conjugated with HRP. **C**, lipid binding profiles of Syt1-Fc fusions using lipid-coated nitrocellulose membranes as shown in Figure 1B. Bound proteins were detected using goat anti-human IgG (H+L) antibody conjugated with HRP. **D,** 2H11 cells were treated with 50 nM docetaxel for 72 hours, or treated with vehicle control (DMSO), and incubated with 50 nM control IgG or PS-specific Fc fusions. Bound Fc fusion was detected using Alexa 488-labeled anti-human IgG (H+L), followed by flow cytometry analyses (MFI, mean fluorescence intensity). **E,** 2H11 cells were incubated with Alexa 647-labeled PS-specific Fc fusions on ice at optimized concentrations (220 nM for Fc-Syt1 and 40 nM for Syt1-Fc-Syt1) to achieve similar levels of surface binding. Cells were then incubated at 37°C for the indicated time points. Surface bound Fc fusions were stripped using 5 mM EDTA and internalized proteins quantitated by flow cytometry analyses. **F** and **G,** 2H11 (**F**) or MDA-MB-231 (**G**) cells were incubated with 50 nM control IgG or PS-specific Fc fusions at 37°C for four hours. Cells were fixed, stained with Cy3/Alexa 555-labeled anti-human IgG (H+L) and LAMP-1-specific antibody followed by Alexa 488-labeled secondary antibody for detecting LAMP-1. Fluorescence images were acquired and Cy3/Alexa 555, Alexa 488 and DAPI are pseudo-colored red, green and blue, respectively, in the overlays. Scale bars: 10 μm (**F**) and 5 μm (**G**). For **D** and **E**, statistically significant differences were analyzed using two-way ANOVA followed by Tukey *post hoc* test (*, $P < 0.05$; **, $P < 0.01$; ***, $P < 0.001$; ****, $P < 0.0001$). Error bars in **D** and **E** represent SEM.

Figure 3. PS-specific PDCs bind to PS in a Ca^{2+}-dependent way, and dissociate from PS in early endosomes prior to lysosomal delivery and disruption of microtubule networks in target cells. **A,** schematic representation of PS-specific PDCs (left panel). The hinge cysteines were reduced and conjugated to four molecules of MMAE (small filled circles). Right panel shows reducing SDS-PAGE analyses of the unconjugated or conjugated PS-specific Fc fusions and control IgG, with molecular weights (MW) shown in kDa on the left. **B,** PS-specific PDCs or MMAE-conjugated control IgG were incubated with PS-coated beads in the presence of the indicated Ca^{2+} concentrations (left panel) or pH levels (right panel). Bead-associated proteins were analyzed using immunoblotting and detection with goat anti-human IgG (H+L) conjugated with HRP. **C,** MDA-MB-231 cells were incubated with 100 nM PS-specific PDCs or MMAE-conjugated control IgG for 30 minutes. Cells were fixed, stained with Alexa 555-labeled anti-human IgG (H+L) and EEA1-specific antibody followed by Alexa 488-labeled secondary antibody for detecting EEA1. Fluorescence images were acquired and Alexa 555, Alexa 488 and DAPI are pseudo-colored red, green and blue, respectively, in the overlays. The endosomes in boxed regions (labeled a and b) are cropped and expanded. Fluorescence intensities along the dotted lines in the overlays for these endosomes are shown in the fluorescence intensity plots. Scale bars: 5 μm (left panels; whole cell images) and 1 μm (right panels; cropped endosomes). **D,** MDA-MB-231 cells were incubated with 50 nM MMAE-conjugated control IgG or PS-specific Fc fusions at 37°C for four hours. Cells were fixed, stained with Alexa 555-labeled anti-human IgG (H+L) and LAMP-1-specific antibody followed by Alexa 488-labeled secondary antibody for detecting LAMP-1. Fluorescence images were acquired and Alexa 555, Alexa 488 and DAPI are pseudo-colored red, green and blue, respectively, in the overlays. Scale bars: 10 μm. **E** and **F,** 2H11 (**E**) and MDA-MB-231 cells (**F**) were treated with 100 nM or 50 nM PS-specific PDCs or MMAE-conjugated control IgG for 10 or 20 hours, respectively. Cells were then fixed, stained with tubulin-specific antibody followed by

Alexa 555-labeled secondary antibody and imaged. Alexa 555 and DAPI are pseudo-colored red and blue, respectively, in the overlays. Scale bars: 15 µm (**E**) and 10 µm (**F**).

Figure 4. PS-specific PDCs inhibit cancer cell growth and survival *in vitro*. PS-positive cancer endothelial cells (2H11), breast cancer cells (T-47D, SK-BR-3 and MDA-MB-231) and prostate cancer cells (LNCaP and 22Rv1) were treated with antibody/protein-drug conjugates at the indicated concentrations. Cell viability following 72 hours (2H11), 96 hours (SK-BR-3, MDA-MB-231 and 22Rv1) or 120 hours (T-47D) is shown. Representative data from two or three independent experiments for each cell line are presented.

Figure 5. Bivalent Fc-Syt1_MMAE inhibits tumor growth *in vivo* and targets multiple PS-positive cells in the tumor tissue. **A,** pharmacokinetic analyses of PS-PDCs in BALB/c SCID mice (n = 5 mice/group). Whole body and blood radioactivities were measured at the indicated time points. **B,** areas under curves in **A** were quantitated and statistically significant differences analyzed using unpaired Student's t-test (****, $P < 0.0001$). **C-E,** BALB/c SCID mice were implanted with MDA-MB-231 (**C** and **E**) or LNCaP (**D**) tumors. Mice (n = 5-6 mice/group) were treated (day 33-60 in **C**, **E** and day 27-59 in **D**) with either unconjugated or MMAE-conjugated Fc fusions at a dose of 1 nmole/mouse (4.1 mg/Kg for Fc-Syt1 or Fc-Syt1_MMAE, 5.6 mg/Kg for Syt1-Fc-Syt1 or Syt1-Fc-Syt1_MMAE) twice per week. PBS was delivered as vehicle control. Tumor volumes (**C, D**) and body weights (**E**) were measured twice per week. Statistically significant differences (Fc-Syt1_MMAE vs PBS in **C**; Fc-Syt1_MMAE vs. PBS or Syt1-Fc-Syt1_MMAE in **D**) at treatment end points were analyzed using one-way ANOVA followed by Bonferroni *post hoc* test (*, $P < 0.05$; ***, $P < 0.001$; ****, $P < 0.0001$). Error bars in all panels represent SEM. **F** and **G**, BALB/c SCID mice bearing MDA-MB-231 tumors were treated (i.p.) with 5 mg/Kg docetaxel 72 and 48 hours before delivery of 1 nmole Fc-Syt1_MMAE. PBS was delivered as vehicle control.

Mice were perfused either 1 hour (**F**) or 24 hours (**G**) post-injection of Fc-Syt1_MMAE. Tumors were dissected out and tissue sections were fixed and stained with Alexa 555-labeled anti-human IgG (H+L), mouse CD31, F4/80 or human Ki-67-specific antibodies followed by Alexa 488-labeled secondary antibodies for detection of CD31/Ki67 and Alexa 647-labeled secondary antibody for detection of F4/80. Confocal images were acquired and Alexa 555, Alexa 488, Alexa 647 and DAPI are pseudo-colored red, green, white and blue, respectively, in the overlays. Scale bars: 50 μm (**F**) and 20 μm (**G**).

Figure 6. Therapeutic effects of Fc-Syt1_MMAE are dependent on PS binding. **A,** reducing SDS-PAGE analyses of the unconjugated or MMAE-conjugated PS-specific Fc fusions and control IgG1 Fc, with molecular weights (MW) shown in kDa on the left. **B,** lipid-coated nitrocellulose membranes were incubated with 2 μg/ml Fc-Syt1 or Fc-Syt1(DN), and bound proteins detected using goat anti-human IgG antibody conjugated with HRP. **C,** 2H11 cells were treated with 50 nM docetaxel for 72 hours, or treated with vehicle control (DMSO), and incubated with 5 μg/ml control Fc, Fc-Syt1 or Fc-Syt1(DN). Bound Fc or Fc fusion was detected using Alexa 488-labeled anti-human IgG (H+L), followed by flow cytometry analyses. Statistically significant differences were analyzed using two-way ANOVA followed by Tukey *post hoc* test (***, $P < 0.001$; ****, $P < 0.0001$). **D,** female BALB/c SCID mice (n = 6 mice/group) bearing MDA-MB-231 tumors were treated with the indicated agents at a dose of 1 nmole/mouse (4.1 mg/Kg for Fc-Syt1_MMAE or Fc-Syt1(DN)_MMAE, 2.6 mg/Kg for Fc_MMAE) twice per week for four weeks (day 28-56) and tumor sizes were measured for a further 2.5 weeks (day 56-74). Statistically significant differences between Fc-Syt1_MMAE and Fc-Syt1(DN)_MMAE treatment groups at the treatment end point were analyzed using one-way ANOVA followed by Bonferroni *post hoc* test (***, $P < 0.001$). **E**, tumors in each group shown in **D** were isolated and photographed. Scale bar: 1 cm. Error bars in **C** and **D** indicate SEM.

Author Manuscript Published OnlineFirst on September 22, 2017; DOI: 10.1158/1535-7163.MCT-17-0092
Author manuscripts have been peer reviewed and accepted for publication but have not yet been edited.

Figure 1

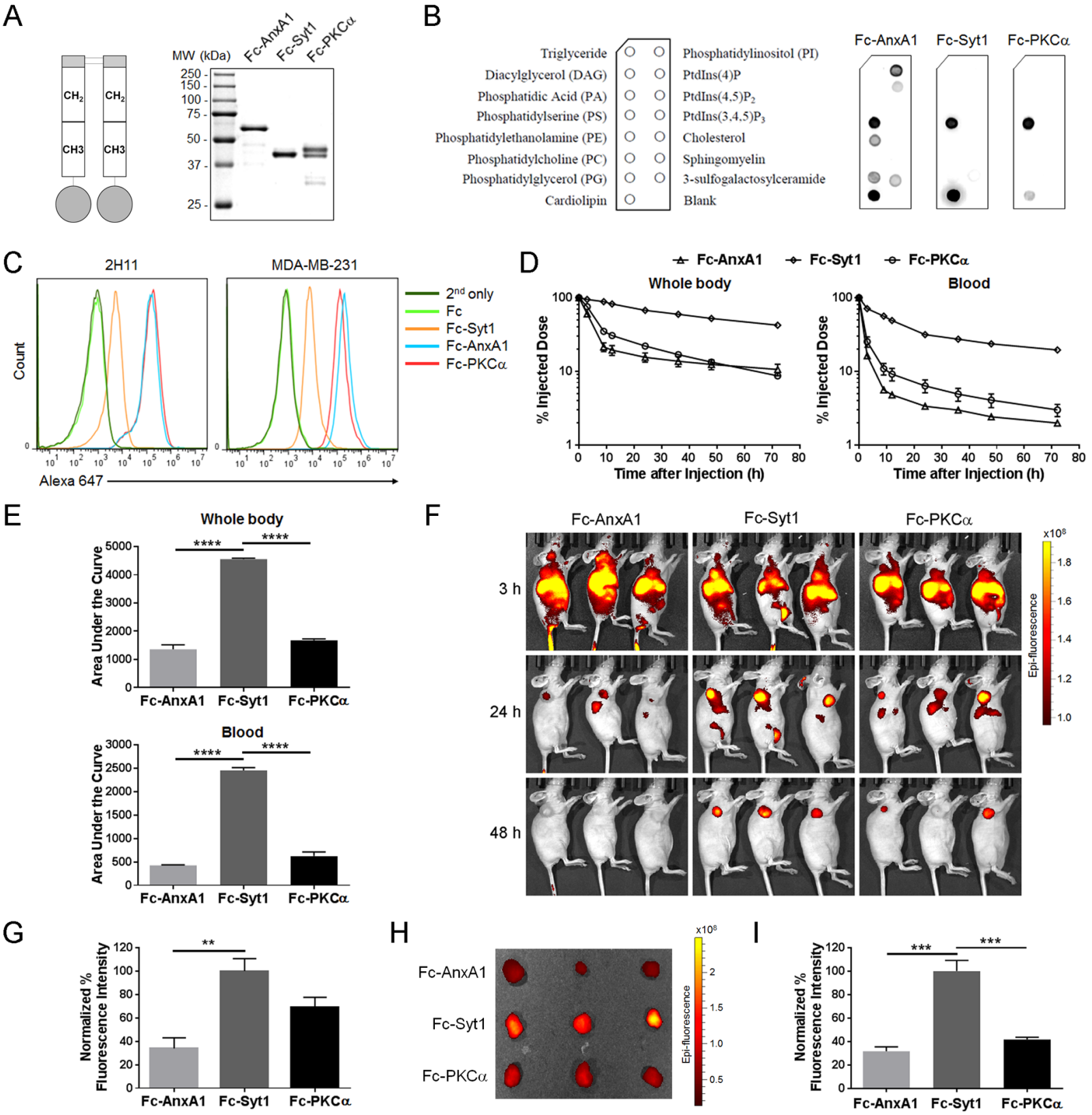

Author Manuscript Published OnlineFirst on September 22, 2017; DOI: 10.1158/1535-7163.MCT-17-0092
Author manuscripts have been peer reviewed and accepted for publication but have not yet been edited.

Figure 2

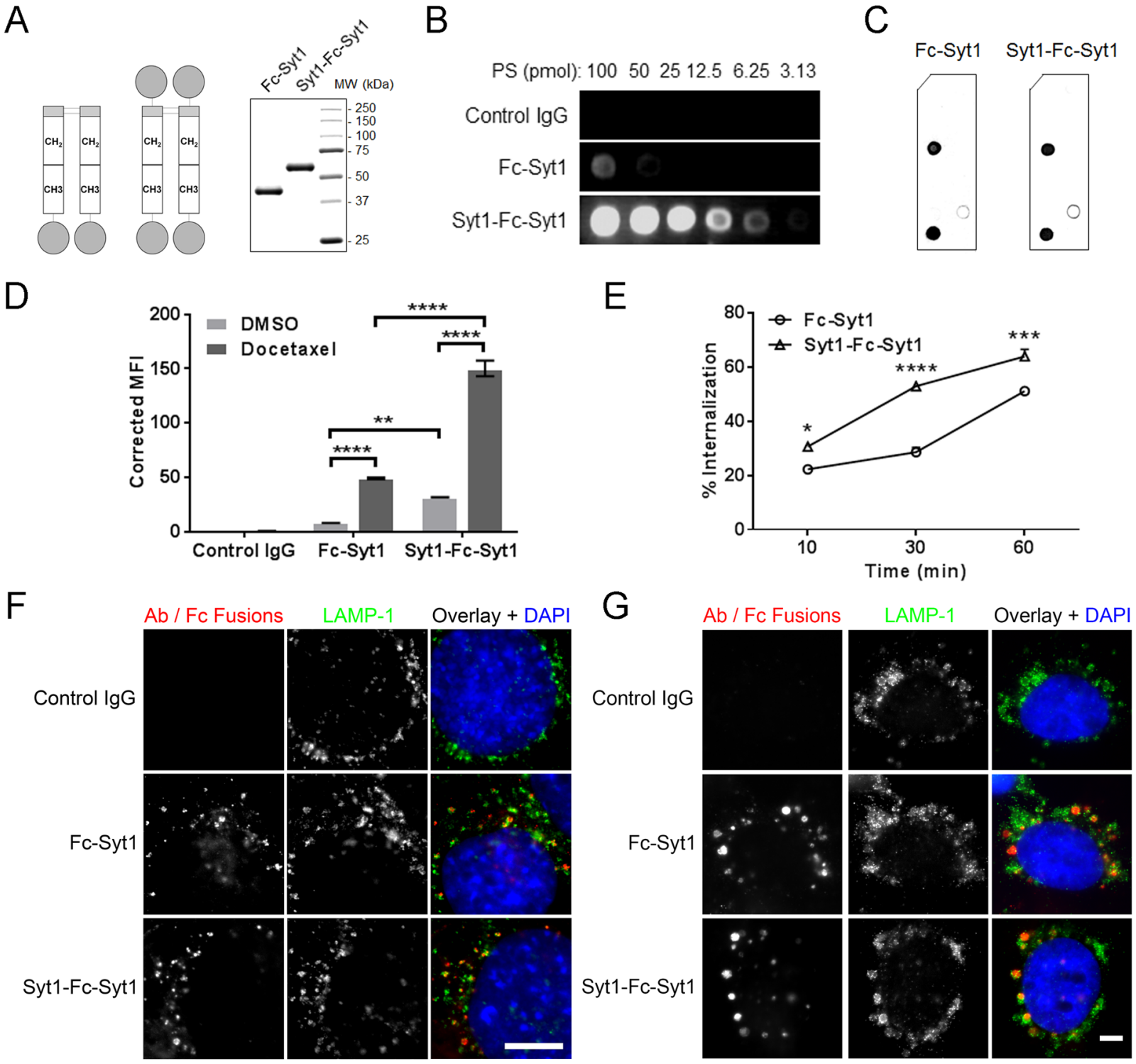

Author Manuscript Published OnlineFirst on September 22, 2017; DOI: 10.1158/1535-7163.MCT-17-0092
Author manuscripts have been peer reviewed and accepted for publication but have not yet been edited.

Figure 3

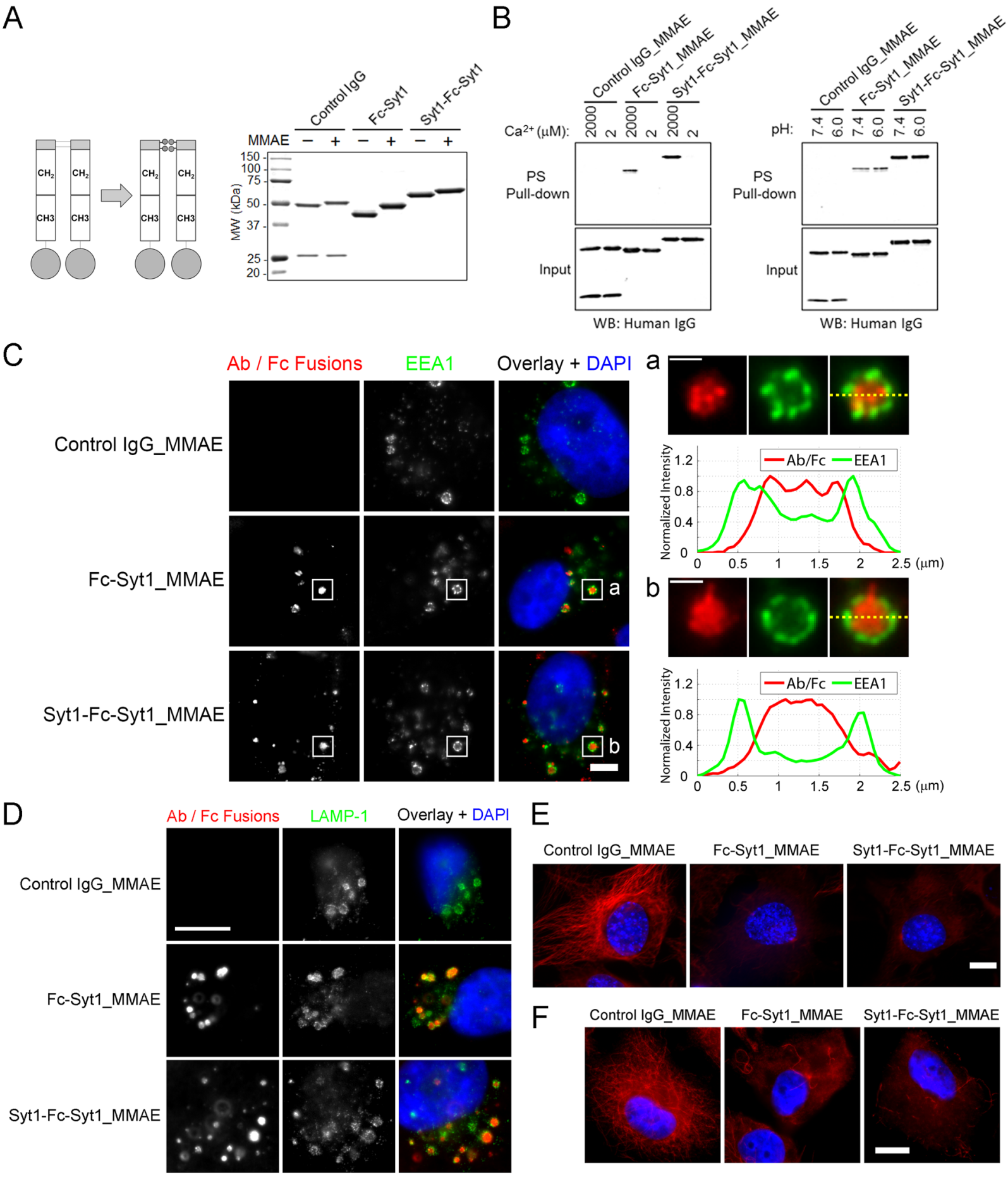

Author Manuscript Published OnlineFirst on September 22, 2017; DOI: 10.1158/1535-7163.MCT-17-0092
Author manuscripts have been peer reviewed and accepted for publication but have not yet been edited.

Figure 4

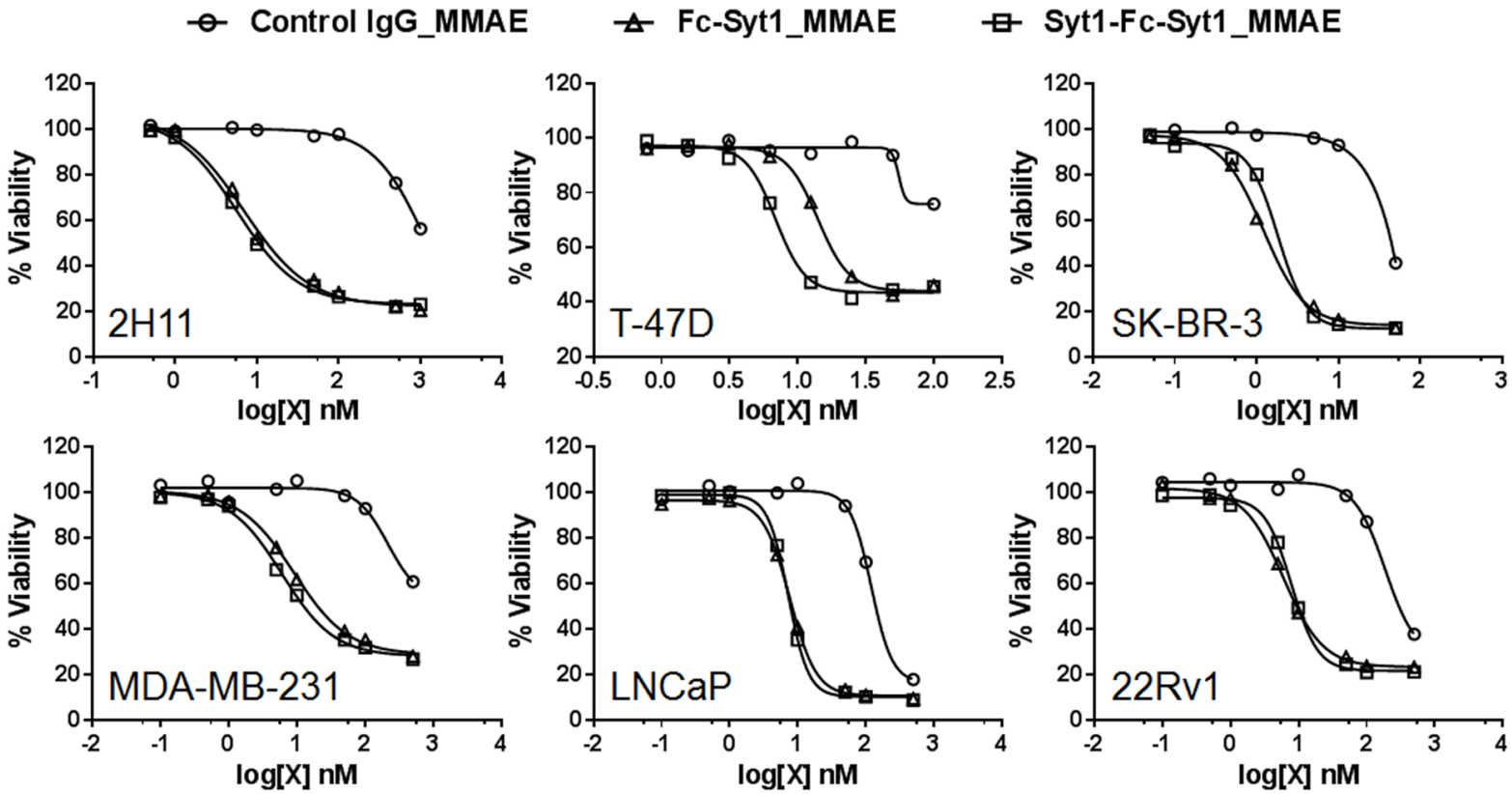

Author Manuscript Published OnlineFirst on September 22, 2017; DOI: 10.1158/1535-7163.MCT-17-0092
Author manuscripts have been peer reviewed and accepted for publication but have not yet been edited.

Figure 5

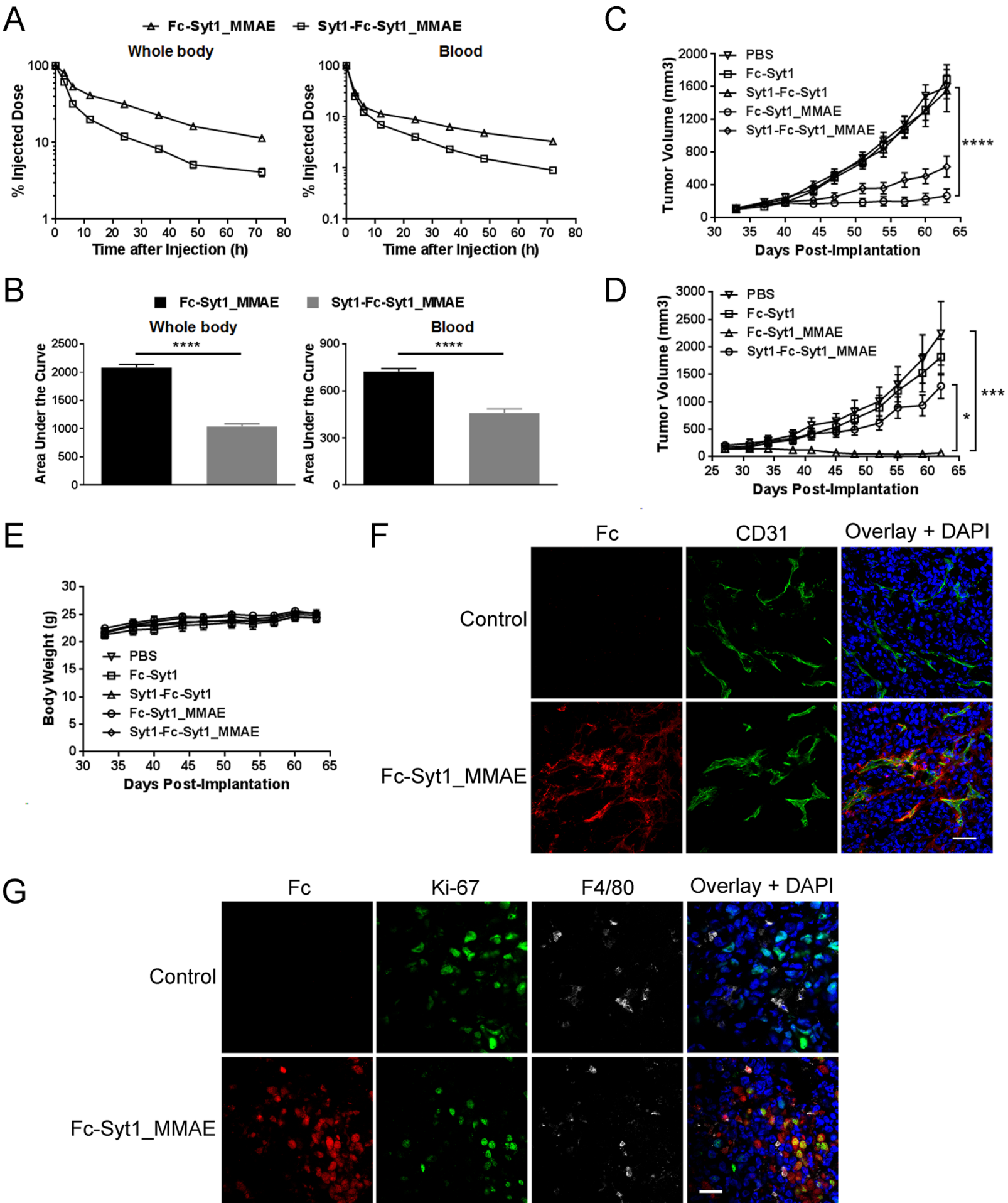

Author Manuscript Published OnlineFirst on September 22, 2017; DOI: 10.1158/1535-7163.MCT-17-0092
Author manuscripts have been peer reviewed and accepted for publication but have not yet been edited.

Figure 6

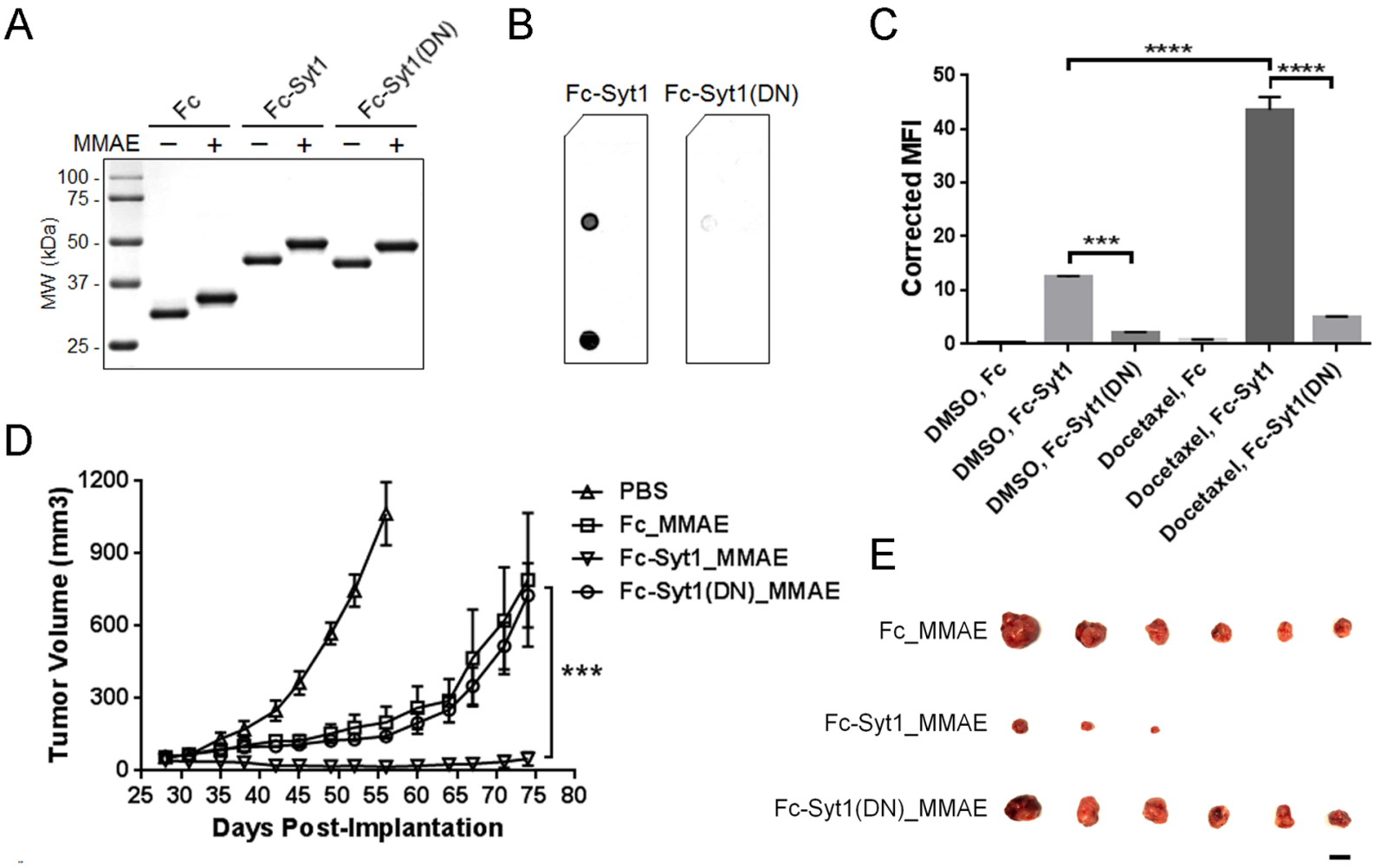

AACR American Association for Cancer Research

Molecular Cancer Therapeutics

Targeting Phosphatidylserine with Calcium-dependent Protein-Drug Conjugates for the Treatment of Cancer

Ran Li, Srinivas Chiguru, Li Li, et al.

Mol Cancer Ther Published OnlineFirst September 22, 2017.